Evidence for fireballs in bipolar HiPIMS plasmas

OPEN ACCESS
IOP Publishing
Plasma Sources Science and Technology
Plasma Sources Sci. Technol. **32** (2023) 025015 (9pp)
https://doi.org/10.1088/1361-6595/acbc97

Evidence for fireballs in bipolar HiPIMS plasmas

Marcus A Law, Francis Lockwood Estrin, Paul M Bryant, Mark D Bowden and James W Bradley*

Department of Electrical Engineering and Electronics, University of Liverpool, Brownlow Hill, Liverpool L69 3GJ, United Kingdom

E-mail: jbradley@liverpool.ac.uk

Received 2 October 2022, revised 7 February 2023
Accepted for publication 16 February 2023
Published 3 March 2023

Abstract

Using laser Thomson scattering (LTS) and 2D optical imaging, a fireball-like discharge is detected during the positive pulse period of bipolar voltage waveforms, for a circular planar unbalanced magnetron with W target operating in argon. These reverse discharges, excited for positive pulse voltages V_{pp} from 200 to 300 V, sit primarily on the discharge centreline. Their establishment is delayed relative to the initiation of the positive pulse, with the delay time shortening with increased V_{pp}: they are clearly attached to the target (anode in this phase) and have lifetimes extending to the end of the positive pulse. LTS measurements of the electron temperature T_e show dramatic electron heating (T_e rises from 1 up to 3 eV) both on the discharge centre line and above the racetrack during the fireball event. This is consistent with greater light intensities from the broad band optical imaging of the discharge. In the fireball phase, the LTS measurements also show greatly reduced election densities (by a factor of 5) in the magnetic trap (directly above the racetrack) compared to the unipolar pulse case. The existence of such anodic fireballs is quite possibly an unwanted effect in bipolar HiPIMS.

Keywords: HiPIMS, bipolar HiPIMS, Thomson scattering, fireball

(Some figures may appear in colour only in the online journal)

1. Introduction

HiPIMS was established over 20 years ago as a form of ionized physical vapour deposition [1]. It has since been used to produce high quality thin films and coatings [2] for a range of applications [2, 3]. The conventional HiPIMS discharge, operates as a series of discrete unipolar pulses delivered to the magnetron cathode target. These pulses typically produce discharge power densities in the range of 0.5–10 kW cm^{-2} but with low duty cycles, between 0.5%–5%, to prevent target overheating [4, 5]. This high instantaneous power, results in plasma densities up to 10^{19} m^{-3} or higher [6, 7] during the HiPIMS on-time pulse leading to a highly ionised sputter flux. This high sputter flux ionisation fraction compared to direct current magnetron sputtering (DCMS) is the primary reason for interest in HiPIMS [2, 4, 8].

Recently, there has been keen interest in a modification to HiPIMS power delivery scheme in which a positive voltage pulse is delivered to the target in the afterglow, a short period after the end of the negative pulse. This technique, first used by Wu *et al* [9], is known as asymmetrical bipolar HiPIMS (BP-HIPIMS). Typically, positive potentials V_{pp} between 50 and 300 V are applied with durations t_{pp} ranging from 10 μs to several 100 μs [10,11].

In the BP-HiPIMS afterglow period, in which the positive pulse is applied, the plasma decays, but substantial

* Author to whom any correspondence should be addressed.

electron densities are still present throughout this period with $n_e \sim 10^{17}$–10^{18} m^{-3} [12, 13]. This plasma will react on application of positive pulse and collective behaviour leads to the applied electric field being shielded in the bulk plasma. This results in the establishment of positive plasma potential (V_p), close to, or matching the target potential, either throughout the bulk [14, 15], or in the form of a potential step (double layer) [16, 17]. Therefore, ions created at these high positive potentials can be accelerated to bombarding energies up to $E \sim eV_p$ at a grounded substrate [10, 18] without the need for the substrate to be biased [9, 19].

BP-HiPIMS has been studied as a means of depositing engineering quality thin films, including Cu [9, 19, 20], Ti [21], diamond like carbon [22, 23], CrN [24, 25] and cobalt oxide [26]. In addition to these materials, the basic processes in BP-HiPIMS discharges have been investigated directly using plasma diagnostic tools. These include non-intrusive techniques such as, time-resolved optical emission spectroscopy [26, 27], laser induced florescence (LIF) [21, 28] and laser Thomson Scattering (LTS) [12]. Intrusive measurements such as Langmuir probes [13, 14], emissive probes [16, 18, 29] and ion energy analysers [11, 15, 16, 30] have also been used. The results of these investigations show ions tend to arrive at the substrate with energies up to a value corresponding to that of the positive pulse voltage V_{pp} [10, 20, 31]. In some cases, it is a moving or stationary double layer in the bulk plasma that appears to be responsible for the ion acceleration e.g. in [17] and [16], however many studies have failed to demonstrate this effect and it is the substrate sheath potential that accelerates ions e.g. in [18, 29].

A potentially unwanted side effect of BP-HiPIMS is the ignition of a reverse discharge during the delivery of the positive pulse [10, 12, 27], indicated by the reappearance of background gas optical emission and elevated electron temperatures. Fast electrons travelling to the positive target and energetic secondary electrons released from the chamber walls have been suggested as candidate sources for the reverse discharge ignition, however, the exact mechanisms are still to be fully explored. The conditions under which they form are similar to those studied by Chauhan *et al* [32] who observed the spontaneous formation of a glowing droplet shaped discharge centred on the target, a discharge they attributed to the fireball phenomena. Similar fireball-like structures have also been observed by Stranak *et al* [33] during dual magnetron sputtering using time-resolved optical imaging. Each target was alternatively pulsed, acting as either cathode or anode. During operation, close to the magnetron with grounded cathode (anode), a bright central column of light was imaged. A fireball is a specific type of anode-plasma interaction, in which ionisation occurs within the anode sheath itself, creating a glowing discharge that expands 100s of Debye lengths from the anode into the bulk; named fireball for its visual appearance [34, 35].

In this contribution, to investigate further the fireball phenomenon in BP-HiPIMS we use non-perturbing incoherent LTS to measure the temporal evolution of electron properties above the race-track and on the centreline with positive pulse magnitudes from 0 to 300 V and durations of 300 μs. The LTS studies are complemented by time-resolved 2D broad band images taken during the positive pulse delivery period, to observe the ignition and characteristic of secondary discharges (fireballs).

2. Experimental arrangement

The experimental arrangement, including the magnetron and diagnostic tools is shown in figure 1 and the LTS system has been described previously in [7]. This set-up was also used recently in an LTS study of the electron properties along the centre-line in BP-HiPIMS discharges [12]. Briefly, the plasma source consists of an unbalanced magnetron (Vtech 150 from GENCOA Ltd) fitted with a 150 mm diameter tungsten target (>99.95% purity). The chamber was evacuated to a base pressure of 2×10^{-3} Pa using a turbomolecular pump backed by a rotary pump. The discharges were ignited at pressures of 1.6 Pa in argon gas (>99.99% purity), powered by an in-house built BP-HiPIMS power supply.

A plot of the typical discharge voltage and current waveforms are shown in figure 2. The negative pulse 'on' time duration was fixed at 50 μs with an 8 μs delay preceding the positive pulse of magnitudes ranging from 0 to 300 V and duration 300 μs. The HiPIMS repetition frequency was 50 Hz. As discussed in a previous publication [12], the inclusion of the positive pulse affects the rise time and peak current observed during the negative pulse. However, this did not affect the overall average discharge power which was measured to be 85 W with a peak power density of 230 W cm^{-2}. From here on in, we define the start of the negative pulse to be $t = 0$ μs.

Figure 3 shows the magnetic field vector directions and magnitudes, measured by a digital Gauss meter (Hirst GM04), together with the LTS scattering volume positions indicated by red crosses. The last closed flux surface is indicated by the white dotted line, highlighting the magnetic trap region. The laser beam propagation was in the target surface plane. Moving the magnetron, up or down relative to the fixed laser beam alignment through the chamber, allowed axial measurements to be performed. For racetrack LTS measurements, the laser beam was focused in scattering volumes on an axial line at radius $r = 48$ mm (above the main erosion groove) at distances 15 mm to 65 mm from the target, in steps of 10 mm. The laser scattering vector ($k = k_s$–k_i) was aligned perpendicular to the magnetrons magnetic B field as depicted in figure 1(b). This corresponds to the component of the electron velocity distribution measured. For centre-line measurements $r = 0$ mm, the laser beam was focused into two scattering volumes at $z = 15$ and 61 mm indicated in figure 3, with an arbitrary scattering vector. The scattering volume recorded on the intensified charge-coupled device (iCCD), measured $3.3 \times 0.17 \times 0.25$ mm^3. Data was accumulated over 600–3000 laser pulses (60–300 s), with longer acquisition time needed to improve the signal to noise ratios of low electron density and high temperatures measured during the positive pulse. The temporal resolution of this system was 5 μs.

A second iCCD camera (Andor istar 334 T), fitted with a 105 mm DG macro lens (sigma EX) was used to take time-resolved images of the broad band optical emission from the

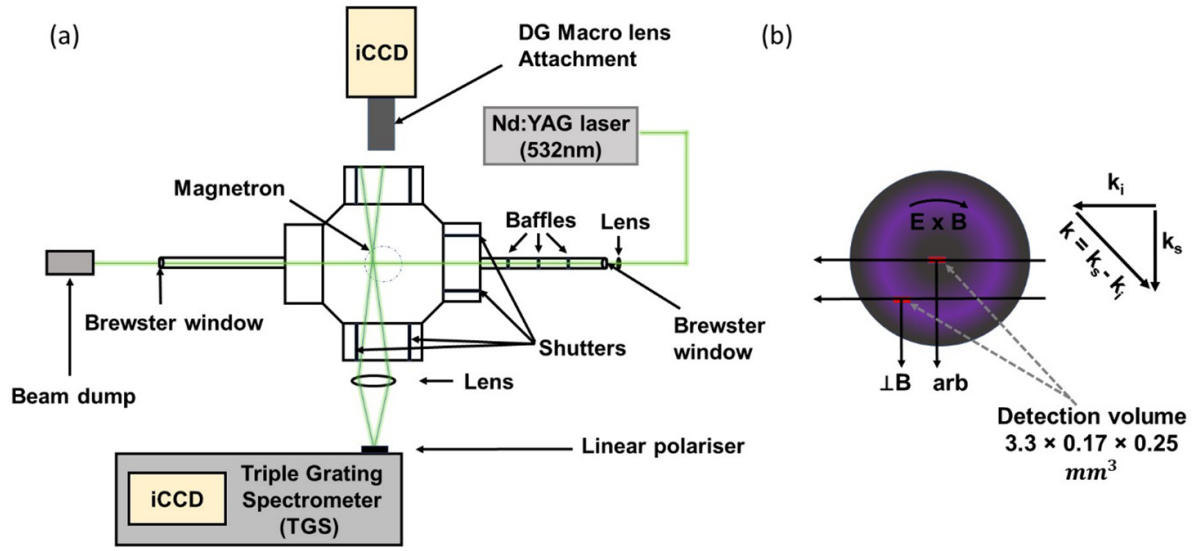

Figure 1. Top view schematic of (a) the experimental apparatus, showing the LTS and 2D optical imaging set up and (b) the LTS scattering detection volumes and resultant scattering vectors, $k = k_s - k_i$. Where k_i and k_s represent the incident and scattered wavevectors respectively.

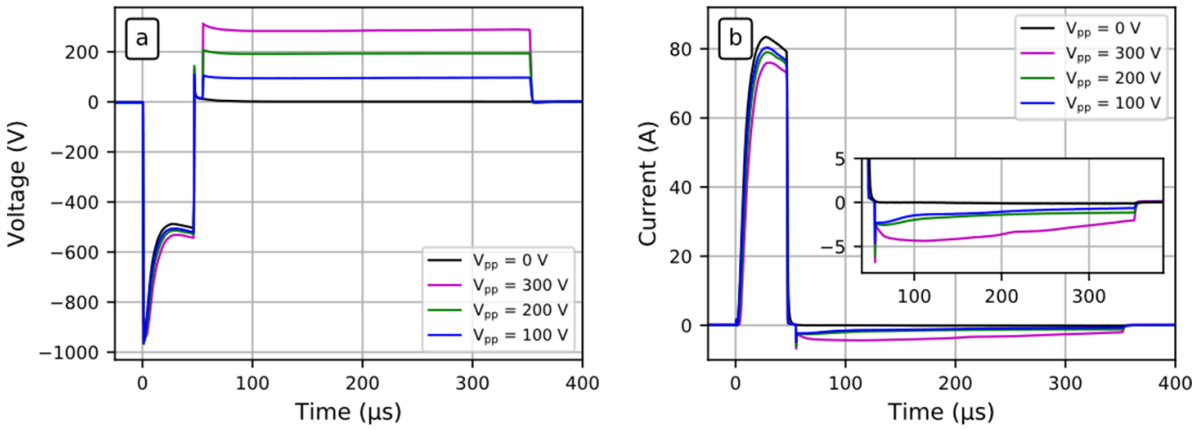

Figure 2. Example discharge voltage (a) and current (b) waveforms. The black line indicates a unipolar pulse of length 50 μs. The coloured lines represent a bipolar pulse with negative on-time of 50 μs with a 300 μs positive pulse with 100, 200, 300 V magnitude. Discharges were operated at 50 Hz with 1.6 Pa argon gas.

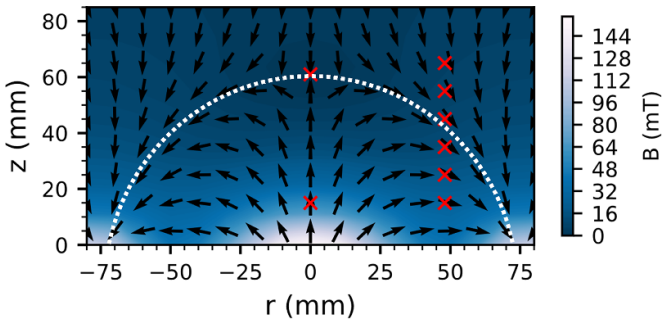

Figure 3. A representation of the magnetic field configuration (field strength and direction) of the magnetron together with the LTS measurement positions (centre of the scattering volumes) highlighted by red crosses. Shown also is the last closed flux surface in white, marking the boundary of the magnetic trap region.

plasma throughout the positive pulse period. The camera had an optical detection range of 200–940 nm and was focused on an object of known size, centred with respect to the magnetron inside the chamber. The resultant images had dimensions of ∼11 × 11 cm captured on the 1024 × 1024 pixel array of the iCCD. Images were taken during the positive pulse with a

gate width of 2 μs and acquired over 2 s (100 HiPIMS pulse periods), with a gain of 2500, synchronised by the transistor-transistor logic (TTL) signal of the HiPIMS generator. Images obtained at different times throughout the discharge are readily comparable to each other; sharing a common intensity scale.

3. The results

The results are presented in two sub-sections below, describing the LTS electron properties and the 2D optical images respectively.

3.1. Temporal evolution of T_e and n_e

To complement the results in our previous publication [12], which show significant electron heating along the discharge centre-line in the positive pulse period, here we present LTS results made in a line above the racetrack. Initially we chose discharges with $V_{pp} = 300$ V and $t_{np} = 50$ and 300 μs, as an extension to our prior BP-HIPIMS study. Figures 4(a) and (b) respectively shows the temporal evolution of electron temperature T_e and density n_e for the six axial measurement positions above the racetrack plotted on the same axis. From figure 4(a), we see a rise in T_e during the positive pulse at all positions. The rise is seen to occur sooner, at positions further from the target, also reaching higher values. T_e peaks at a value of 2.2 eV at the $z = 65$ mm whilst at $z = 15$ mm the temperature only reaches 0.25 eV. This indicates we have a region of hot plasma some distance away from the target.

The corresponding density plots, figure 4(b), shows a significant drop in the middle of the magnetic trap during this heating phase. Positions close to and far from the target show the least density reduction in the positive pulse.

To investigate the difference in electron parameter behaviour between positions on the centreline and above the racetrack we have made LTS measurements of T_e and n_e at four different locations as shown in figure 5.

We choose two positions on the centre-line ($r = 0$) one close to the target at $z = 15$ mm and the other downstream $z = 61$ mm, see figures 5(a)–(d), these results are also presented in [12]. The equivalent two positions above the racetrack ($r = 48$ mm) are inside the magnetic trap at $z = 15$ mm and outside the trap at $z = 65$ mm, figures 5(e)–(h). Two discharge cases are considered, BP-HiPIMS with $V_{pp} = 300$ V and the unipolar case $V_{pp} = 0$ V.

In terms of electron heating, the main result is that during the positive pulse, electron heating can be seen at all positions on the centre line (figures 5(a) and (b)), however above the racetrack this phenomenon is seen outside the magnetic trap (figure 5(f)). Close to the target inside the magnetic trap, little heating is observed (figure 5(e)). On the centreline the application of the positive pulse does not change the electron density n_e compared to the unipolar case (figures 5(c) and (d)). However, above the racetrack n_e is significantly reduced (figures 5(g) and (h)).

To obtain a broader picture of the heating phenomenon and electron density reduction above the racetrack on application of the positive pulse, LTS measurements have been made for positive voltages V_{pp} of 100, 200 and 300 V at $r = 48$ mm and $z = 35$ mm. These are shown in figure 6, together with the unipolar $V_{pp} = 0$ V case.

Similar to the centre-line results, there was no measured T_e increase for the $V_{pp} = 100$ V case during positive pulse delivery. The $V_{pp} = 200$ V case shows a T_e increase towards the end of the positive pulse. The timings of this T_e rise is in line with what was measured centre-line (figure 5 and in [12]). The temperature rise occurs some 100 μs sooner with $V_{pp} = 300$ V than the 200 V case. With $V_{pp} = 300$ V the fall in electron density in the trap is most dramatic. With application of $V_{pp} = 100$ V there is little or no change in the n_e decay profile compared to the unipolar case. It is clear that for voltages greater 100 V the electrons become significantly denuded with measured values down by a factor of 5 of the comparable unipolar case.

3.2. 2D optical imaging of the reverse discharge

It has been suggested in [10, 12, 27, 29] that during the positive pulse of a BP-HiPIMS plasma, a reverse discharge ignites. This reverse discharge has significant similarities to the fireball phenomena as mentioned in section 1 above. Here we present direct evidence of this phenomenon, observed using time-resolved broad band 2D optical imaging. Figure 7 shows images taken at four time-steps during the $V_{pp} = 300$ V discharge. These images were taken over a gated 2 μs exposure window with 2 s total acquisition time, over which 100 plasma pulses are averaged. In the images we also show the magnetic field direction (shape) and the positions at which the LTS measurements were made are marked.

In general, we see that as the reverse discharge (fireball) develops it takes the shape of a dewdrop anchored on the target centre. Note, the target is now acting as an anode. This discharge is squeezed to the centre line by the lobes of the trap magnetic field. Early images ($t \leqslant 220$ μs), not shown, reveal a homogeneous dark chamber with relatively low optical output, until ignition of the fireball occurred at $t \geqslant 220$ μs.

Figure 7(a) shows an image taken in the relatively early stages of the ignition of this secondary discharge ($t = 225$ μs), where a bright central region begins to be illuminated. A relatively dark region also appears in the magnetic trap, as the electron density in this region has been depleted (see figure 4).

Figure 7(b) shows the brightest observed broad band emission during the reverse discharge, taken at $t = 240$ μs. Evident in this image are the glowing wings, extending from the central column of light emission, with analogous shape to the magnetron B-field. This bright region is due to magnetised electrons which follow the field lines as they are attracted to the now positive target, stimulating emission via collisions with the background gas. Figure 7(c) shows time step $t = 280$ μs, where the plasma extends further downstream in the z direction, illuminating more of the chamber and giving the reverse discharge a more triangular shape. Figure 7(d) shows a time period just before the positive pulse termination ($t = 350$ μs), where the electron temperature measured by LTS has dropped from its initial peak. This is apparent in the image, as the intensity of

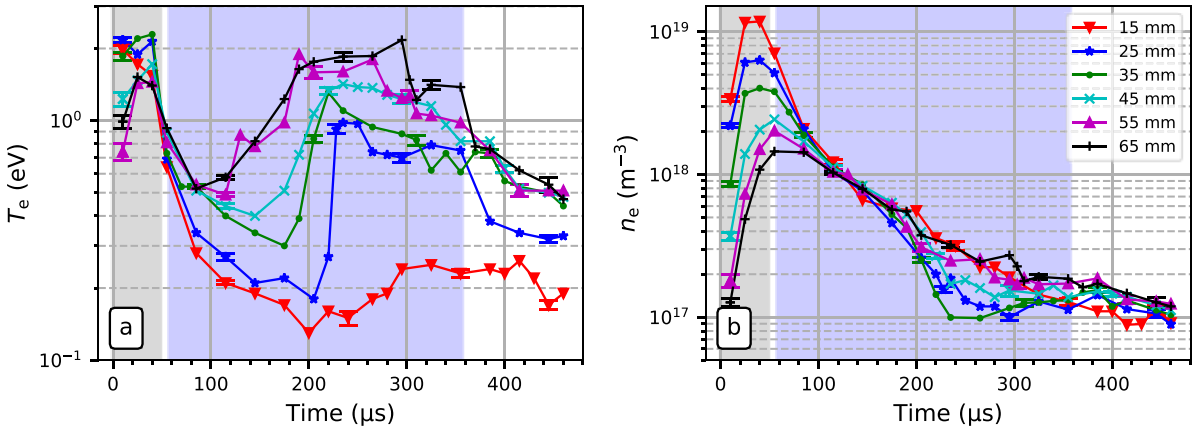

Figure 4. Plots of (a) the electron temperature T_e and (b) electron density n_e versus time at six axial positions above the racetrack ($r = 48$ mm) with for a positive pulse of $V_{pp} = 300$ V. The negative pulse duration of $t_{np} = 50$ μs is shown as the grey region, while the positive pulse duration of $t_{pp} = 300$ μs is shaded blue. The operating pressure was 1.6 Pa.

the glow has decreased and the plasma ceased its extension in the z direction. The fireball returns to the original dewdrop shape.

4. Discussion

In a previous publication [12] using LTS, significant electron heating was observed above the target centreline with the application of bipolar positive voltages $V_{pp} \geqslant 200$ V. Some of those results are shown in this contribution. Investigations here have been extended to include measurements above the racetrack. As shown in figure 6, the application of a 200–300 V positive pulse, leads to a rise in electron temperature above the racetrack; similar to what is seen along the centreline. Close to the target however, this rise is only modest. The density of electrons within the magnetic trap during this heating period drops significantly compared to the unipolar (falling by a factor 5). No such depletion in n_e is observed on the centreline of the system.

LTS measurements for $V_{pp} = 300$ V show a rise in electron temperature, within the positive pulse at each measured position, although the rise in T_e at $z = 15$ mm is notably stunted. Along the centreline, the increase in T_e occurs at $t \sim 180$ μs, for both $z = 15$ mm and 61 mm. However, the start of the T_e rise above the racetrack is dependent on distance. The $z = 65$ mm shows the earliest increase, at $t \sim 120$ μs with latest increase at $z = 15$ and 25 mm, occurring at $t \sim 200$ μs. This means, by the time the fireball ignites ($t = 220$ μs), T_e has risen in all locations. T_e continues to rise till it reaches a maximum at $t = 240$ μs, this peak correlates with the brightest intensity image as measured by the iCCD camera, strongly linking the fireball ignition to rising electron temperatures. When a $V_{pp} = 200$ V positive pulse is used, the increase in T_e occurs ~ 100 μs later than the $V_{pp} = 300$ V case. The observed ignition found from 2D imaging (not shown here), reflects the same delay.

A fireball is defined as an anode-plasma interaction in which a discharge originates on the anode and extends into the bulk plasma [34, 35]. 2D imaging reveals such a structure is present during the positive pulse of our BP-HiPIMS system. During the positive voltage phase, a bright dewdrop structure forms, with intense light emission stemming from the centre-line, shaped by the magnetic field topology of the magnetron. Relatively dark regions appear outside the centreline close to the target, inside the magnetic trap. LTS measurements showed that these areas have significant density reduction. Close to the target above the racetrack, little electron heating is observed.

Given that both optical output and the T_e of the fireball reduce during the positive pulse, it might be assumed the fireball is not self-sustaining. However, iCCD images of a bipolar pulse with, $t_{np} = 50$, $V_{pp} = 300$ V, $t_{pp} = 2$ ms (not include in this paper) show that the fireball is visible right up to the pulse termination. A self-sustaining fireball was observed by Chauhan *et al* [32] using a type-2 unbalanced with 7.5 mTorr argon gas, with a constant +300 V direct current (DC) positive bias applied to the target. Both of these suggest that the fireball is capable of self-sustaining despite the observed cooling and dimming.

It is interesting that, although significant electron heating is observed downstream of the target within the magnetic trap ($15 < z < 45$ mm), with application of 200 and 300 V positive voltages, the broad band emission from this region of the plasma is weak, with the bright fireball existing primarily on the centre line.

We hypothesise that secondary electrons, created at the vessel walls through ion bombardment, are accelerated through the wall sheath potential into the bulk plasma. For these hot electrons to enter the magnetic trap, they must cross the field lines, which effectively insulate the bulk plasma from the racetrack region of the target. This low thermal conduction path for electrons leads necessarily to a temperature gradient, with cooling from the outer regions ($z = 45$ mm) of the trap towards to the target ($z = 15$ mm) as can been deduced from figure 4(a). This may explain the reduced optical emission close to the target (which is acting as a thermal and conductive sink). By contrast, along the centre-line electrons are

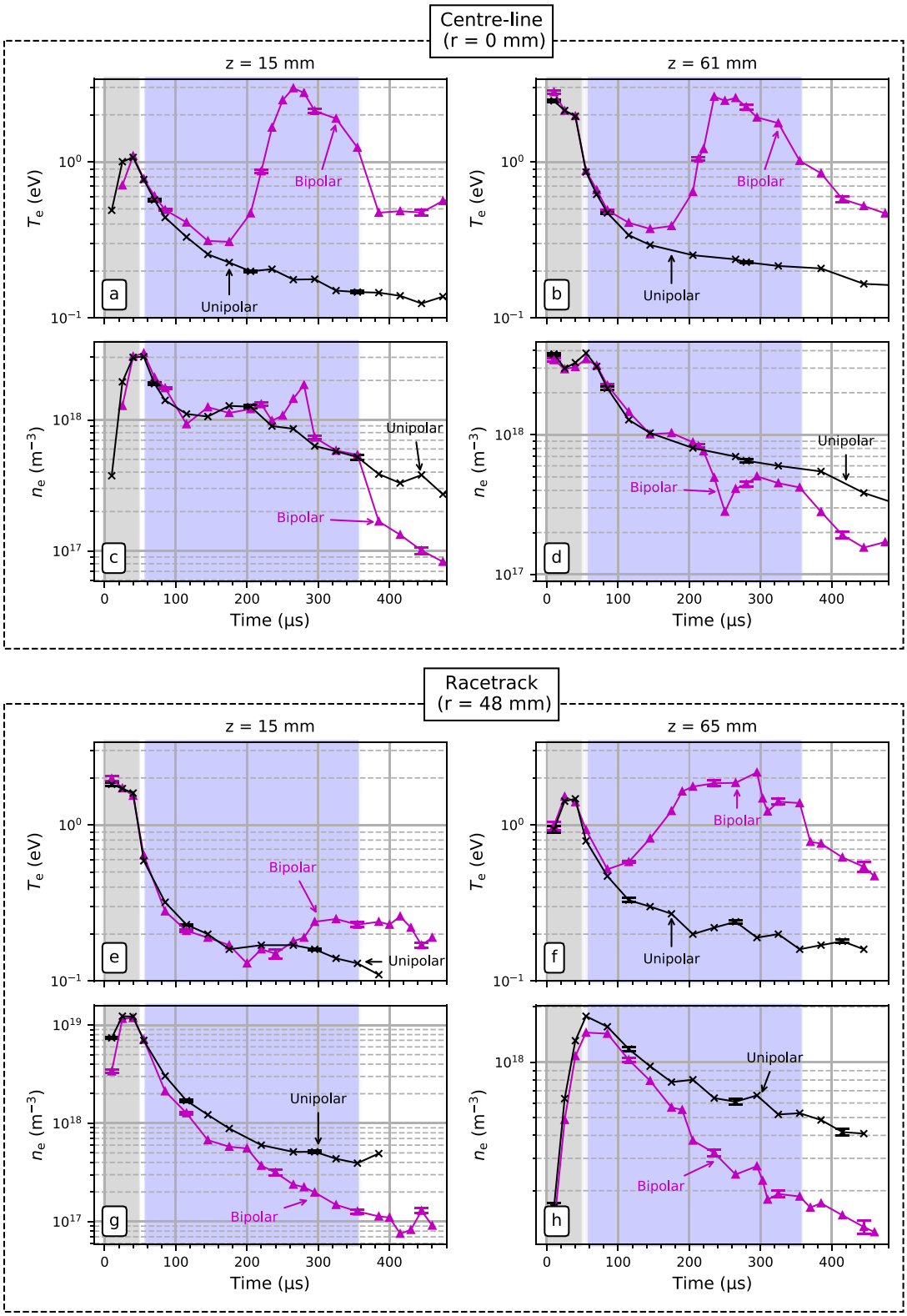

Figure 5. Plots of electron density n_e and electron temperature T_e versus time at comparable axial positions on the centre-line and above the race track groove, for $V_{pp} = 300$ V (triangle symbol) and the comparable unipolar (cross symbol) pulses. (a,c,e,g) $z = 15$ mm, (b, d, f, h) $z = 61, 65$ mm.

unimpeded by the magnetic field and no electron temperature gradient is observed. Relatively high electron temperatures along the centre-line may be responsible for the relatively strong optical emission from this region.

One possibility for hot electrons in the trap at distances far from the target (not associated with secondary electrons from the wall) may be due to the existence of gradients or double layers in the electric potential structure, established

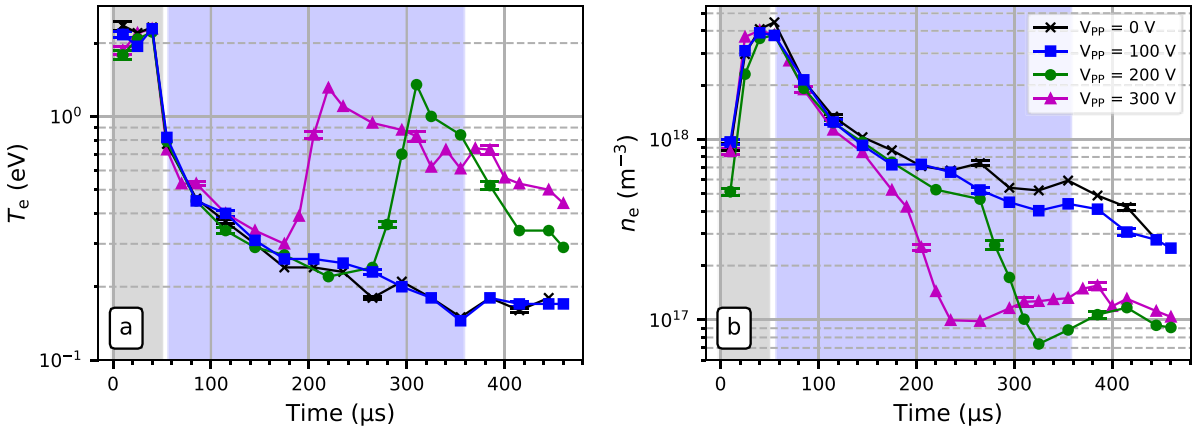

Figure 6. Plots of (a) the electron temperature T_e and (b) electron density n_e versus time measured in the magnetic trap ($r = 48$ mm, $z = 35$ mm) for $V_{pp} = 0$, 100, 200 and 300 V with all the other operating conditions the same as in figure 2.

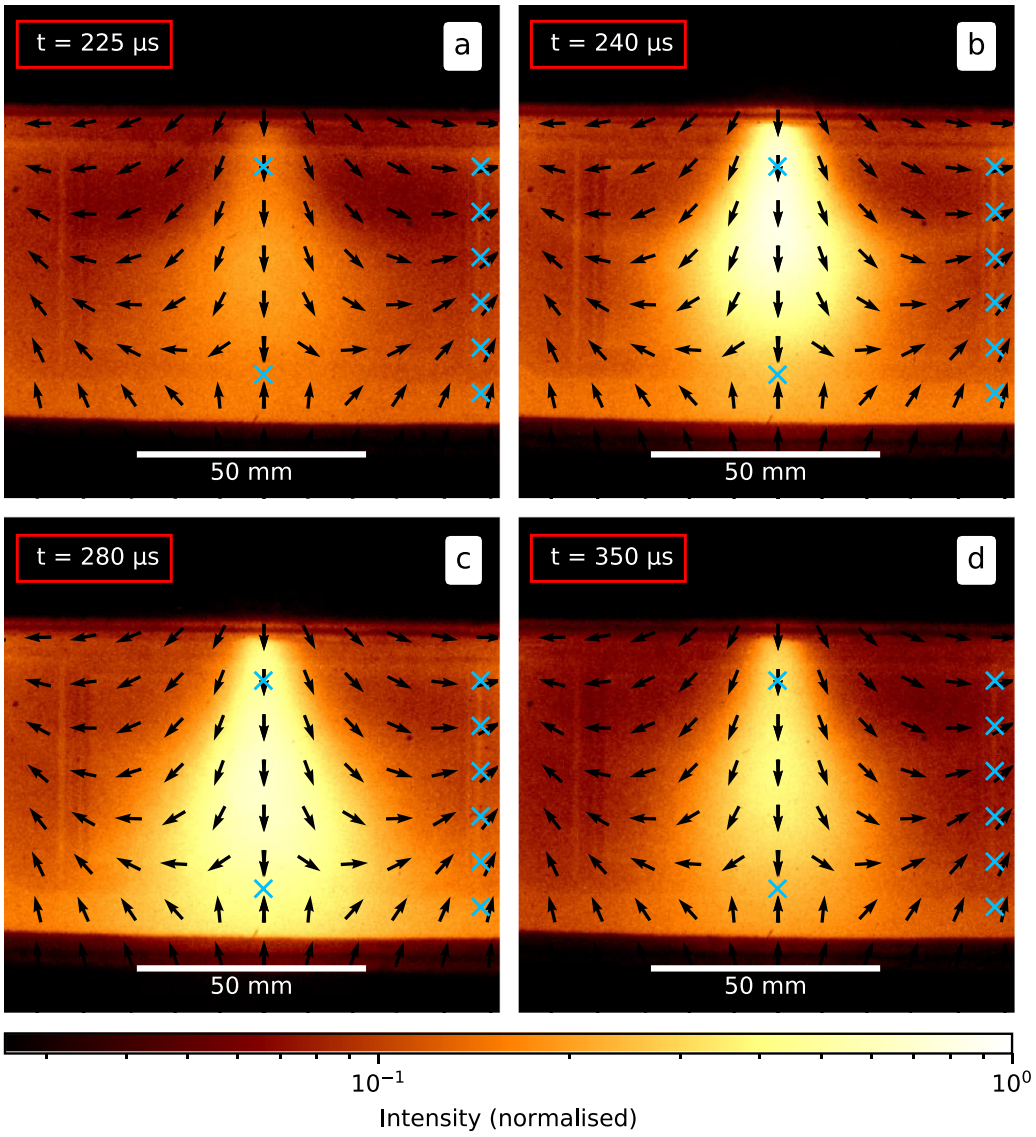

Figure 7. ICCD images taken during the positive pulse of a bipolar discharge of $V_{pp} = 300$ V at ((a) 225 μs, (b) 240 μs, (c) 280 μs and (d) 350 μs) after the initiation of the negative pulse. The magnetron is mounted vertically, facing downward. The magnetron anode ring protrudes ~7 mm from the target surface.

by ionisation in the anode sheath; the mechanism responsible for fireball discharges [34, 35]. Measurements of the plasma potential by emissive probe in this scenario show little evidence of steps or gradients in V_p, so we believe electron heating in the trap and centreline is a result of energetic secondary electron release from the vessel walls as the plasma potential V_p rises rapidly everywhere in the plasma close to the value of V_{pp} set by the operator as described in [12].

Whatever the cause, this reverse discharge (fireball) may be detrimental in industrial thin film production since its effect on the sputter disposition process is yet unclear. The depletion of electron density, shown in figure 6 would indicate that ions are being removed from the bulk plasma to maintain quasi-neutrality. These ions, leaving the plasma will be accelerated to a grounded substrate. Given the delay between the appearance of the fireball and the end of the negative pulse, ion bombardment will be performed by background gas, not the target material. This may enhance the ion-assisted process [36, 37], however it is likely to have a detectable effect on the deposited films, increasing ion power flux to the growing film. However, there is evidence from optical emission studies that elevated plasma potentials in positive pulse period lead to some wall sputtering [12]. The development of a burning fireball on the discharge centreline rooted to the target, may result in a source of unwanted metallic species.

5. Conclusions

Using LTS and broad band 2D optical imaging, we have shown direct evidence of the ignition of a discharge with characteristics (length and shape) of a fireball during the positive pulse of bipolar HiPIMS. In our case (V_{pp} = 200–300 V, t_{pp} = 300 μs) there is significant electron heating (up to 3 eV) at all measured positions on the discharge centreline and within the magnetic trap, at distances greater than 15 mm from the target. Significant electron depletion is observed above the racetrack at all distances, reducing by a factor of 5 of the comparable unipolar pulse. This however, does not occur at the centreline.

The fireball does not form immediately on the initiation of the positive pulse, it appears visually only after T_e has increased at all positions. With increasing V_{pp} the T_e rise happens sooner within the positive pulse and the rise in T_e is directly correlated to the ignition of the fireball, observed from broad band optical imaging. The fireball is shaped by the magnetic field structure of the magnetron and sits primarily on the magnetron centreline, attached to the positive target.

This ignition of a fireball discharge, during the positive pulse delivery, may well be an unwanted side effect in BP-HIPIMS configuration. The exact mechanisms that produce and sustain the fireball are still not fully understood: It could be for instance due to the generation of energetic electrons by bulk plasma electric fields above the target centre, close to the anode or, from hot electrons produced via secondary electron emission from the walls.

Data availability statement

All data that support the findings of this study are included within the article (and any supplementary files).

Acknowledgments

This work was supported by the Engineering and Physical Sciences Research Council (Grant EP/L01663X/1)

ORCID iDs

Marcus A Law https://orcid.org/0000-0002-2165-5503
Francis Lockwood Estrin https://orcid.org/0000-0002-1922-1124
Mark D Bowden https://orcid.org/0000-0003-4128-4823
James W Bradley https://orcid.org/0000-0002-8833-0180

References

[1] Kouznetsov V, Macák K, Schneider J M, Helmersson U and Petrov I 1999 A novel pulsed magnetron sputter technique utilizing very high target power densities *Surf. Coat. Technol.* **122** 290–3
[2] Gudmundsson J T, Brenning N, Lundin D and Helmersson U 2012 High power impulse magnetron sputtering discharge *J. Vac. Sci. Technol.* A **30** 030801
[3] Lundin D and Sarakinos K 2012 An introduction to thin film processing using high-power impulse magnetron sputtering *J. Mater. Res.* **27** 780–92
[4] Helmersson U, Lattemann M, Bohlmark J, Ehiasarian A P and Gudmundsson J T 2006 Ionized physical vapor deposition (IPVD): a review of technology and applications *Thin Solid Films* **513** 1–24
[5] Lundin D, Minea T and Gudmundsson J T 2020 Introduction to magnetron sputtering *High power impulse magnetron sputtering: fundamentals, technologies, challenges and applications* (Amsterdam: Elsevier) 1–48
[6] Bohlmark J, Gudmundsson J T, Alami J, Latteman M and Helmersson U 2005 Spatial electron density distribution in a high-power pulsed magnetron discharge *IEEE Trans. Plasma Sci.* **33** 346–7
[7] Ryan P J, Bradley J W and Bowden M D 2019 Comparison of Langmuir probe and laser Thomson scattering for plasma density and electron temperature measurements in HiPIMS plasma *Phys. Plasmas* **26** 1–6
[8] Kudlácek P, Vlcek J, Burcalová K and Luka J 2008 Highly ionized fluxes of sputtered titanium atoms in high-power pulsed magnetron discharges *Plasma Sources Sci. Technol.* **17** 025010
[9] Wu B, Haehnlein I, Shchelkanov I, McLain J, Patel D, Uhlig J, Jurczyk B, Leng Y and Ruzic D N 2018 Cu films prepared by bipolar pulsed high power impulse magnetron sputtering *Vacuum* **150** 216–21
[10] Kozák T, Pajdarová A D, Čada M, Hubička Z, Mareš P and Čapek J 2020 Ion energy distributions at substrate in bipolar HiPIMS: effect of positive pulse delay, length and amplitude *Plasma Sources Sci. Technol.* **29** 065003
[11] Viloan R P B, Zanáška M, Lundin D and Helmersson U 2020 Pulse length selection for optimizing the accelerated ion flux fraction of a bipolar HiPIMS discharge *Plasma Sources Sci. Technol.* **29** 125013
[12] Law M A, Lockwood Estrin F, Bowden M D and Bradley J W 2021 Diagnosing asymmetric bipolar HiPIMS discharges

using laser Thomson scattering *Plasma Sources Sci. Technol.* **30** 105019
[13] Hippler R, Cada M and Hubicka Z 2020 Time-resolved Langmuir probe diagnostics of a bipolar high power impulse magnetron sputtering discharge Time-resolved Langmuir probe diagnostics of a bipolar high power impulse magnetron sputtering discharge *Appl. Phys. Lett.* **116** 064101
[14] Pajdarová A D, Kozák T, Hubička Z, Čada M, Mareš P and Čapek J 2020 Plasma parameters in positive voltage pulses of bipolar HiPIMS discharge determined by Langmuir probe with a sub-microsecond time resolution *Plasma Sources Sci. Technol.* **29** 085016
[15] Walk F, Valizadeh R and Bradley J W 2022 Ion energy analysis of a bipolar HiPIMS discharge using a retarding field energy analyser *Plasma Sources Sci. Technol.* **31** 065002
[16] Tiron V and Velicu I L 2020 Understanding the ion acceleration mechanism in bipolar HiPIMS: the role of the double layer structure developed in the after-glow plasma *Plasma Sources Sci. Technol.* **29** 15003
[17] Keraudy J, Viloan R P B, Raadu M A, Brenning N, Lundin D and Helmersson U 2019 Bipolar HiPIMS for tailoring ion energies in thin film deposition *Surf. Coat. Technol.* **359** 433–7
[18] Han M, Luo Y, Li L, Gu J, Xu Y and Luo S 2021 Optimizing the ion diffusion in bipolar-pulse HiPIMS discharge (BP-HiPIMS) via an auxiliary anode *Plasma Sources Sci. Technol.* **30** 095016
[19] Viloan R P B, Helmersson U and Lundin D 2021 Copper thin films deposited using different ion acceleration strategies in HiPIMS *Surf. Coat. Technol.* **422** 127487
[20] Velicu I L, Ianoş G-T, Porosnicu C, Mihăilă I, Burducea I, Velea A, Cristea D, Munteanu D and Tiron V 2019 Energy-enhanced deposition of copper thin films by bipolar high power impulse magnetron sputtering *Surf. Coat. Technol.* **359** 97–107
[21] Britun N, Michiels M, Godfroid T and Snyders R 2018 Ion density evolution in a high-power sputtering discharge with bipolar pulsing *Appl. Phys. Lett.* **112** 234103
[22] Santiago J A, Fernández-Martínez I, Kozák T, Capek J, Wennberg A, Molina-Aldareguia J M, Bellido-González V, González-Arrabal R and Monclús M A 2019 The influence of positive pulses on HiPIMS deposition of hard DLC coatings *Surf. Coat. Technol.* **358** 43–49
[23] Tiron V, Ursu E-L, Cristea D, Munteanu D, Bulai G, Ceban A and Velicu I-L 2019 Overcoming the insulating materials limitation in HiPIMS: ion-assisted deposition of DLC coatings using bipolar HiPIMS *Appl. Surf. Sci.* **494** 871–9
[24] Batková S, Čapek J, Rezek J, Čerstvý R and Zeman P 2020 Effect of positive pulse voltage in bipolar reactive HiPIMS on crystal structure, microstructure and mechanical properties of CrN films *Surf. Coat. Technol.* **393** 125773
[25] Tiron V, Ciolan M A, Bulai G, Cristea D and Velicu I L 2021 Effect of pulsing configuration and magnetic balance degree on mechanical properties of crn coatings deposited by bipolar-hipims onto floating substrate *Coatings* **11** 1526
[26] Hippler R, Cada M, Stranak V and Hubicka Z 2019 Time-resolved optical emission spectroscopy of a unipolar and a bipolar pulsed magnetron sputtering discharge in an argon/oxygen gas mixture with a cobalt target *Plasma Sources Sci. Technol.* **28** 115020
[27] Hippler R, Cada M and Hubicka Z 2020 Time-resolved diagnostics of a bipolar HiPIMS discharge *J. Appl. Phys.* **127** 203303
[28] Michiels M, Leonova K, Godfroid T, Snyders R and Britun N 2022 Magnetic field topology for altering ion density in bipolar sputtering *Appl. Phys. Lett.* **121** 051603
[29] Zanáška M, Lundin D, Brenning N, Du H, Dvořák P, Vašina P and Helmersson U 2022 Dynamics of bipolar HiPIMS discharges by plasma potential probe measurements *Plasma Sources Sci. Technol.* **31** 025007
[30] Avino F, Manke F, Richard T and Sublet A 2021 Afterglow dynamics of plasma potential in bipolar HiPIMS discharges *Plasma Sources Sci. Technol.* **30** 115015
[31] Viloan R P B, Gu J, Boyd R, Keraudy J, Li L and Helmersson U 2019 Bipolar high power impulse magnetron sputtering for energetic ion bombardment during TiN thin film growth without the use of a substrate bias *Thin Solid Films* **688** 137350
[32] Chauhan S, Ranjan M, Bandyopadhyay M and Mukherjee S 2016 Droplet shaped anode double layer and electron sheath formation in magnetically constricted anode *Phys. Plasmas* **23** 013502
[33] Stranak V, Bogdanowicz R, Drache S, Cada M, Hubicka Z and Hippler R 2011 Dy-namic study of dual high-power impulse magnetron sputtering discharge by optical emission imaging *IEEE Trans. Plasma Sci.* **39** 2454–5
[34] Scheiner B, Barnat E V, Baalrud S D, Hopkins M M and Yee B T 2017 Theory and simulation of anode spots in low pressure plasmas *Phys. Plasmas* **24** 113520
[35] Baalrud S D, Scheiner B, Yee B T, Hopkins M M and Barnat E 2020 Interaction of biased electrodes and plasmas: sheaths, double layers, and fireballs *Plasma Sources Sci. Technol.* **29** 053001
[36] Pachchigar V, Ranjan M and Mukherjee S 2019 Role of hierarchical protrusions in water repellent superhydrophobic PTFE surface produced by low energy ion beam irradiation *Sci. Rep.* **9** 8675
[37] Ashok S, Kräutle H and Beneking H 1984 Effect of argon ion implantation dose on silicon Schottky barrier characteristics *Appl. Phys. Lett.* **45** 431–3